THE SUBSURFACE CHARACTERISTICS OF PEARLITIC RAIL STEELS FOLLOWING SERVICE IN UK

F. A. M. Alwahdi A. Kapoor[*] and F. J. Franklin[*]

Department of Mechanical Engineering, University of Omar Almukhtar, P. O. Box 390 M
Elbyada, Libya, E-mail: faragalwahdi@hotmail.com
[*]School of Mechanical and Systems Engineering, University of Newcastle, Stephenson
Building, Claremont Road, Newcastle upon Tyne, NE1 7RU, UK

الملخص

المواد المطيلة تتعرض لتشوه مرن في مناطق التلامس والمناطق القريبة منها مما يتسبب في انفعالات كبيرة لها تأثير بالغ على عميلة البرى على قضبان السكك الحديدية. حيث معظم مثل هذه المواد غالبا يحدث لها انهيار عندما تكون تحت تأثير مستويات عالية من الانضغاط ويكن تصرفها تحت تلك الظروف لا يمكن دراسته بالاختبارات القياسية للمواد عند الضغط الجوي. الدراسة الحالية تهدف إلى اختبار خمسة قضبان من السكك الحديدية المستعملة والجديدة والتي تستخدم لدى هيئة السكك الحديدية الانجليزية. تم عرض النتائج على هيئة منحنيات استجابة إجهاد وانفعال ناتجة من اختبار مواد تحت انضغاط هيدروستاتيكي والتي تعتبر نمطية لظروف تلامس العجلات مع قضبان السكك الحديدية. كما تم أيضا عرض تغيرات الصلادة وإجهاد القص مع العمق تحت سطح القضبان الساخنة بالإضافة إلى البنية المجهرية للمواقع التي تمت دراستها.

ABSTRACT

Ductile materials commonly exhibit plastic deformation at and near the contact surface and their flow behavior at large strains has a clear effect on wear resistance. These materials almost always fail while under high levels of compression, but behaviour under these conditions cannot be investigated by standard materials tests at atmospheric pressure. In this work, the characteristics of the near-surface region of one new and four used rails are examined using samples taken from rails that have been in service in UK. The results are presented as stress-strain response curves from the materials under high hydrostatic compression conditions, which are typical of rail-wheel contacts. In addition, shear strain and hardness variation with depth below the worn rail surface are presented, along with micrographs of the sites examined. A thin white surface layer, frequently called white etching layer (WEL), with high hardness (up to 1040 HV) was observed on the surface of one of the used rails. These results have application in the modelling of rail failure by wear and in modelling rolling contact fatigue crack initiation, and can therefore be used to improve rail maintenance planning and risk assessments.

KEYWORDS: Strain hardening, Rail steel, Pearlitic steel, Microhardness, White-etching layer

INTRODUCTION

Knowledge of the mechanical properties of the surface layer is important for optimising the materials selection for rails. It is established that rolling-sliding contact between the surfaces of ductile materials is often accompanied by severe plastic deformation localized to a small volume of material adjacent to the surface [1, 2]. The depth of plastic flow ranges from a fraction of a millimeter to as much as 15 mm [3]. Such depth increases with severity of track curvature and hence contacts forces but decreases with increase in rail material hardness [4]. The processes of wear debris formation have been shown to be closely related to the magnitude and distribution of these subsurface strains [5]. In ductile materials, the strains at the worn surfaces are much larger than deformations in conventional engineering structures and the wear resistance correlates well with the surface hardness rather than the bulk hardness [6]. To increase understanding of the relationship between wear and plastic deformation, the mechanical properties on the surface layer of one new and four used pearlitic rail steels were investigated. The hardness of the surface layer was determined by performing microhardness tests on sections through the worn surface with a Vickers indenter. Optical micrographs of longitudinal and transverse cross-sections of typical used rails display a heavy plastic deformation on the worn surface. This deformation does not occur in one cycle but is accumulated incrementally over hundreds of thousands of cycles by ratchetting. As the material accumulates deformation, the ductility is exhausted and the material fails as tiny flaws appear in the surface of the material. This failure mechanism is termed ratcheting failure (RF) and is different than low cycle fatigue (LCF). These are two hypotheses to estimate the life: one treats RF & LCF to be competitive so that whichever first produces failure governs the life [7]. The other treats them as additives. However the max difference in the two approaches is of the order of 50% if a Miner's summation value is utilized [8].

Ratcheting failure has been used to model wear. In the Dynarat [9] ratchetting wear model the wearing material is divided into many layers and each layer accumulates shear strain (γ) dependant on its stress and the current shear yield stress (shear yield stress changes with strain in work hardening or softening materials). Any surface layer that accumulates a critical shear strain (γ_c) is said to have failed, and if it is at the surface it is removed from the simulation as wear debris. The model has been extended [10] by having lateral variation of material properties across a mesh of rectangular elements or "brick" rather than simply dividing the material into layers. This model has been used to investigate wear rate and crack initiation life and depends on both initial mechanical properties and work hardening properties of the material. These data are collected in the current tests which present results from metallographic examination and hardness surveys on longitudinal and transverse cross sections of one new and four used pearlitic rail steels. Strain and hardness distributions under the worn surface of each material are determined. This work is intended to supply input data for the computer simulation of wear, (Dynarat model) and crack initiation [11]. The ultimate aim is to develop these models with predictive capabilities over a broad range of operation conditions and material properties to aid maintenance planning.

WHITE ETCHING LAYER

During the metallographic examination it was observed that a thin white surface layer, frequently called white etching layer (WEL), with 10 to 40 μm thicknesses was present on some of the rail samples. The WEL reached hardness values up to ~1040

HV. Different investigations [12-15] suggest that there is no common composition or structure for all white layers. The white etching layers are named as a consequence of their resistance toward metallographic etching and thus their featureless appearance under optical microscopes. It is assumed that owing to friction, temperatures higher than 700°C arise at the wheel-rail contact, leading to austenite formation and dissolution of carbides. Subsequently, after the wheel-rail contact has moved away, rapid cooling of the surface layer causes the martensite transformation. WEL is generally thought to be detrimental to the life of the rail, so to remove it the surface of the rails has to be ground.

PROCEDURE

The four rails (P1, P2, P3 and P4) were supplied by AEAT Rail, Derby UK following their removal from UK Main Line Passenger Track. The rails were all installed in 1993 and removed in the first half of 2003. An unused rail (P5) was also supplied. The chemical compositions of the rail steels are given in Table (1).

Table 1: Chemical compositions of the five rail steels (wt.%)

Chemical composition	Rail code				
	P1	P2	P3	P4	P5
Carbon	0.56	0.73	0.78	0.80	0.75
Sulphur	0.028	0.014	0.014	0.014	0.026
Phosphorus	0.019	0.023	0.019	0.019	0.014
Silicon	0.18	0.21	0.19	0.15	0.23
Manganese	1.07	0.85	0.83	0.84	0.98
Chromium	0.02	0.03	0.02	0.02	0.03
Nickel	<0.02	<0.02	<0.02	<0.02	<0.02
Molybdenum	< 0.02	< 0.02	< 0.02	< 0.02	<0.02

Specimens were cut from the head and gauge corner of rails. The position of the specimens in relation to the rail is shown in Figure (1). Four samples were cut from each rail allowing both longitudinal and transverse deformation to be observed. These samples were top transverse (TT), top longitudinal (TL), gauge transverse (GT) and gauge longitudinal (GL). The samples were mounted in Bakelite, diamond polished down to a particle size of 1 μm and etched with a 2% nital solution (nitric acid in ethanol) for 10 seconds to reveal the microstructure. This is the standard metallographic preparation technique for pearlitic rail steel.
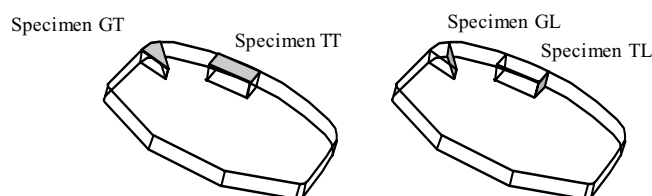
Figure 1: A schematic representation of a rail head, showing the locations of specimens relative to the rail section.

Optical micrographs of the specimens were taken to reveal shear deformation in the region between the rail surface and the undeformed material deeper into the rail. Shear deformation is central to the ratcheting mechanism of plastic strain accumulation within the rail, and is one of the key properties that can be revealed by examination of a worn rail steel. Rigney et al. [6] noticed that some microstructural features such as grain

boundaries, twin boundaries and lamellae can be utilized to provide information about the deformation characteristics of layers below the surface and optical microscopy was sufficient for this purpose. The total plastic shear strains were estimated by measuring the angle (θ) of the deformed grain boundaries and deformed pearlitic lamellae relative to the normal to the contact surface. Measurements were taken on micrograph images that were transferred to a PC equipped with the image analysis software (g3data) [16]. These optical images were taken by using POLYVAR-MET/2.GA/E-85/01 camera to reveal the shear deformation in the region between the worn surface and the undeformed material deeper into the rail. Figure (2) shows a schematic representation of this method. Shear strain (γ_p) was calculated as the tangent of the angle (θ). This method of shear strain measurement was used by Tyfour et al. [17] and was found to give a reasonably accurate measure of strain. Cimenoglu [18] used the same method to determine effective plastic strain from the shear angle of pearlite bands at depths less than 20 μm from the worn surface. Alpas et al. [1] also used a similar technique to measure displacement of a marker platelet, inserted in a test specimen surface, during sliding contact testing.
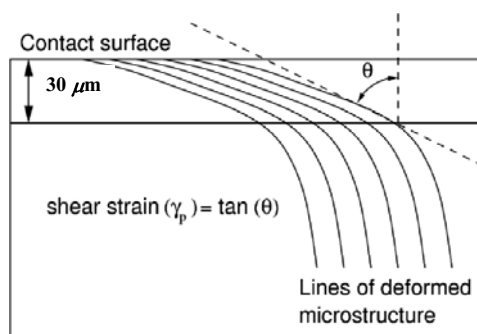
Figure 2: Shear strain measurement technique. Deformation of the steel produces alignment of its microstructure in the direction of deformation. Measuring the angle of these deformation lines at 30 μm below the surface gives the shear strain at this depth. Further depths are sampled in a similar way [17].

Hardness surveys of the sectioned specimens were carried out with a LECO M-400 MVK-E micro-hardness tester. A maximum load of 10g was applied at each measurement point to obtain the Vickers hardness number. Such a light load was used to allow adjacent readings to be closely spaced. Readings were taken at depths from 30 to 1500 μm below the contact surfaces. To ensure accurate results, the separation of each indent from other indents and from the specimen surface was always greater than 30 μm (i.e. greater than three times the largest expected indent diagonal length) in accordance with British Standard BS427 (1990). Further readings were taken further below the surface of the rail materials of P1 and P2 (up to 27mm) with 50kg load and corresponding wider separation of indents. In some cases, problems were associated with determining the exact depth below the worn surface owing to the irregular surface morphology, though these regions were generally avoided, as were regions of the surface with large amounts of impressed oxide or transferred debris.

RESULTS

Subsurface microstructure

Considering rail P1, examination of specimen GL (gauge corner, longitudinal deformation) revealed shear deformation under the worn surface with a visible depth of between 60 and 110 μm depending on the position across the specimen. In specimen TL (top of head, longitudinal), the deformed layer was still present, but with visible thickness reduced to between 50 and 90 μm, as shown in Figure (3). Although wear would continually remove surface material, thereby reducing the remaining depth of plastic deformation, plastic deformation can be in a steady state in only a few contact passes, so wear will not have significantly influenced the depth of deformation observed.
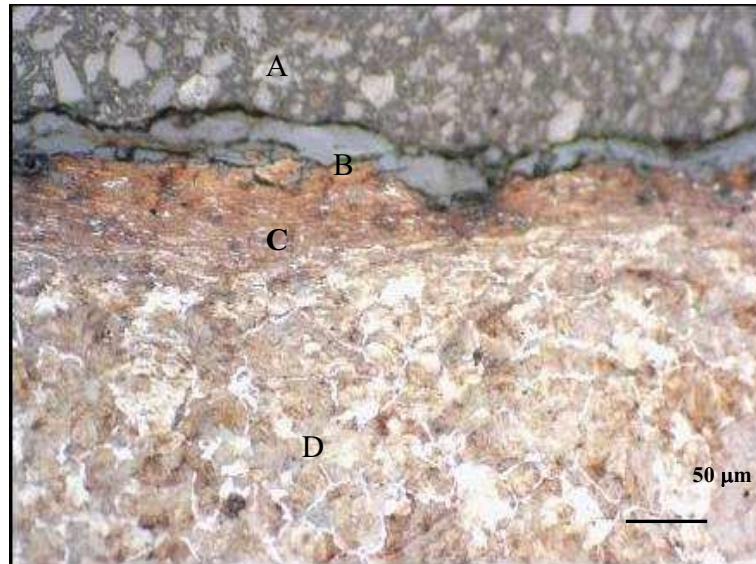
Figure 3: Optical micrograph of longitudinal section of rail gauge face site (TL) for rail P1. Moving down the picture there is (A) sample mounting material, (B) rail surface debris, (C) plastically deformed steel, and (D) at the bottom the undeformed steel microstructure is visible.

Taking rail P2, visible deformation reaches less deeply into the material than for the P1 rail. Figure (4) illustrates this deformation in the longitudinal direction for the rail gauge face and also shows a small surface breaking crack in the rail. Visible deformation reaches depths up to 40 μm, below which the rail steel appeared to be undeformed. The difference in depth to which plastic deformation has reached in the P1 and P2 rails is reflected in the shear strain vs. depth curves for the very near surface material plotted in Figure (5). From these results, it is clear that the strain accumulation of rail P2 was lower than for rail P1. Rail P2 also showed less plastic deformation at the surface. This could be a result of rail grinding in track, whereby the surface layer of the rail head is removed (this is the material in which the build up of plastic deformation is highest) and fresh material is exposed to the running wheel.
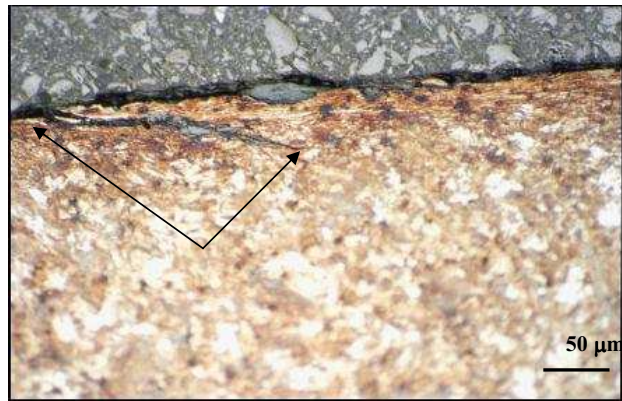
Figure 4: Optical micrograph of longitudinal section of the rail gauge face (GL) for rail P2. Moving down the picture there is sample mounting material, the rail surface containing a crack (with mouth and tip indicated by arrows) at the bottom the undeformed steel microstructure is visible.
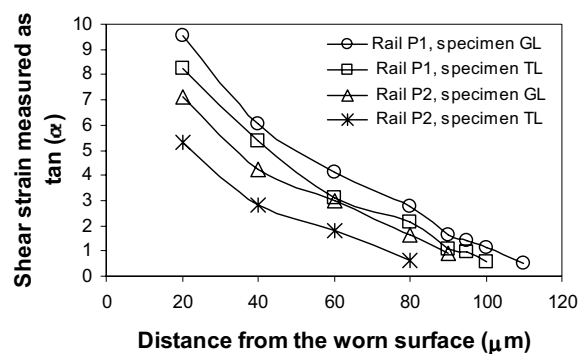
Figure 5: Longitudinal plastic shear strain vs. depth, very close to the surface of the P1 and P2 rails. Specimen TL indicates the top of rail sample and specimen GL indicates the gauge face sample.

Plastic deformation reaching a depth of 150 μm was observed in the surface of rail P3 at the top transverse specimen. The plastic deformation in the gauge corner of the rail can be seen in Figure (6a) where the plastic deformation exceeded the depth of that found on the rail head by 30 μm. The longitudinal cross section through rail P3 revealed a white etching layer (WEL) in patches of about 10μm thickness, although the thickness was not uniform over the width of the rail surface (see Figure (6b)). The WEL reached a maximum depth of approximately 40 μm and contained small cracks over the full width of the running surface. The composition and the structure of the WEL remains the subject of research, but investigations [12-15] suggest that there is no common composition or structure for all white etching layers.

(a)
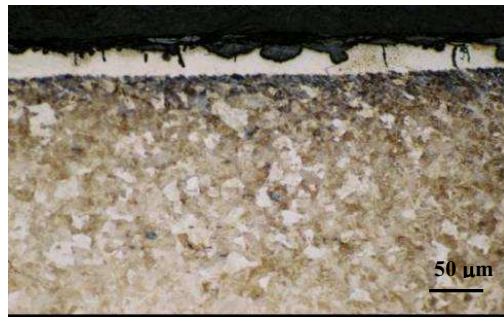
(b)

Figure 6: Microstructure of P3 rail material under the worn surfaces; (a) transverse section of the rail gauge (GT), moving down the picture there is sample mounting material and the plastically deformed layer below the running surface; (b) longitudinal section of the top rail face (TL), moving down the picture there is sample mounting material, a narrow band of WEL and the deformed steel microstructure is visible.

Metallographic examinations of longitudinal sections from rail P4 revealed shear deformation beneath the worn surface of the gauge corner (specimen GL). As shown in Figure (7a), the microstructure of the steel consisted of ferrite and cementite bands elongated in the rolling direction. The variation of shear strain with depth from the worn surface of both rails P3 and P4 are plotted in Figure (7b), where it can be seen that the plastic deformation at the gauge corner is greater than that at the crown of each rail, and that the deformation extended to larger depth. Figure (8) shows the gauge longitudinal cross section (specimen GL) of the unused rail sample (P5). It shows two layers: a decarburised surface layer (~120 m thickness) with small grain size, and a bulk material layer with a microstructure characteristic of pearlitic, with no deformation. The decarburised layer was very soft and contained large amount of ferrite. There is a strong tendency for carbon to be lost from the surface of steel during heat treatment and this is one of the oldest most persistent problems in ferrous production metallurgy. Decarburisation lowers resistance to wear and localized patches of decarburisation can lead to soft spots. Weakening of the surface as a result of decarburisation may favour the initiation of fatigue cracks [19].

Figure 7a: Optical micrograph of longitudinal section of the rail gauge face (specimen GL) for rail P4. Moving down the picture there is sample-mounting material; large deformed steel microstructure is visible
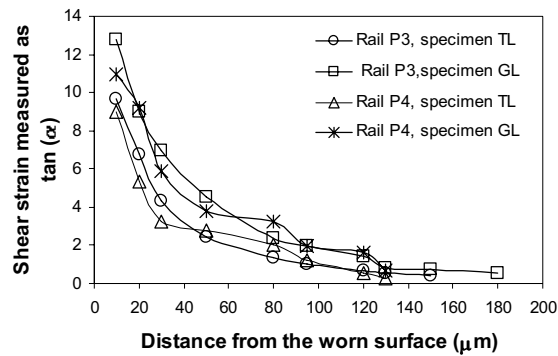
Figure 7b: The variation of shear strain with distance from the worn surface for rails P3 and P4.

Figure 8: Optical micrograph of longitudinal section of the rail gauge face (GL) for new rail P5. Moving down the picture there is sample mounting material, top rail surface containing a small grain size with large amount of ferrite and the bulk material microstructure.

Subsurface hardness

Profiles of hardness from the surface down into the undeformed (by visual inspection) material are shown in Figure (9a) for all the samples examined. The P1 and P2 rail heads had a hardness of 210HV and 245HV respectively. The increase in hardness at the surface of each rail steel (around 1.8 and 1.6 times the bulk rail head hardness respectively) can be attributed to work hardening. Although the hardness differential between the materials was reduced as both materials hardened close to the surface, the ranking of the steels remained the same throughout.
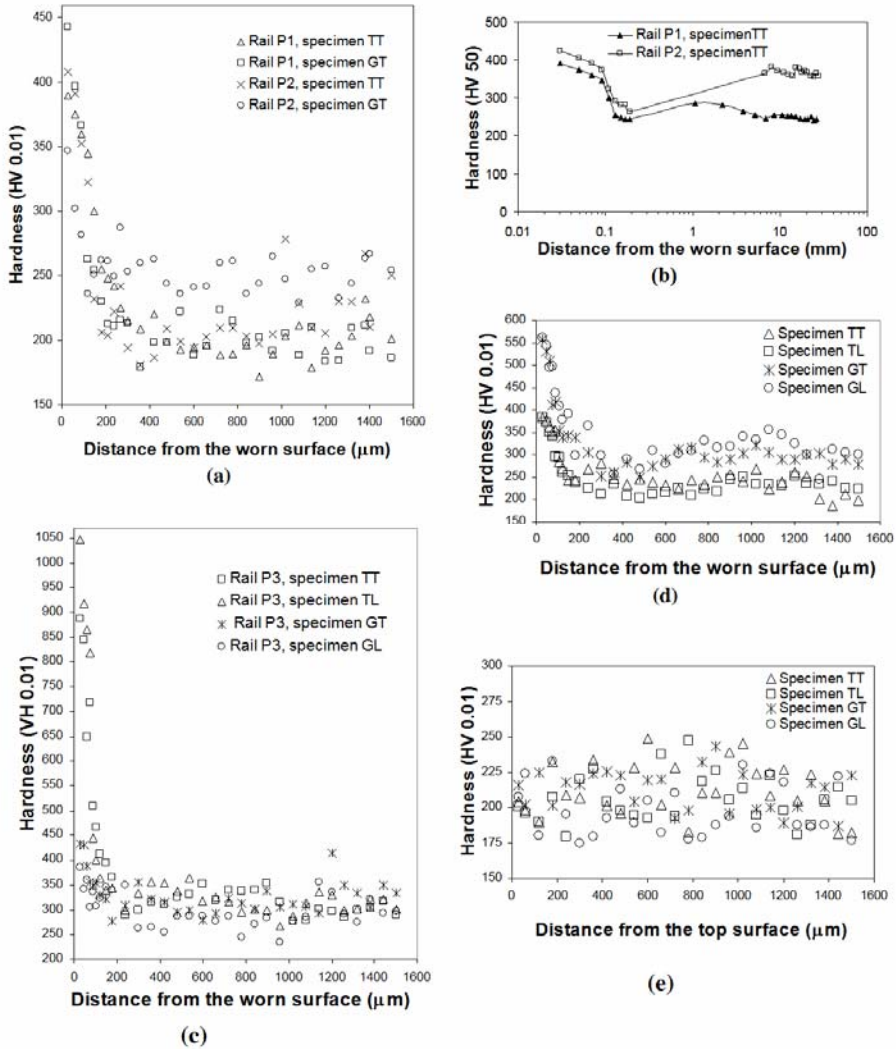
Figure 9: Rails hardness variation with depth (a) of rails P1 and P2 with 10g load and 1.5 mm depth (b) of rails P1 and P2 with 50 kg load and 27 mm depth. (c) of rail P3 (d) of rail P4 (e) for the new rail P5.

Looking at the hardness profile at greater depth for the P2 steel, an increase in the spread (250-270 HV) of the results was observed. Figure (9b) shows the hardness variation with depth up to 27 mm for P1 and P2 rail steel samples. Near surface measurement are taken from Figure (9a) (with 10g load) but a 50kg load is used at greater depths. A log scale is used to ensure all data are visible. Hardness tests at greater depths revealed a region of increased hardness at between 1 and 10 mm deep. This is to be expected, and is produced by the action of the wheel contact as a whole. The near surface plastic deformation is produced by the action of micro roughness [20].

A discontinuity existed between the 10g and 50kg measurements. In part this was due to severe cracking, around which hardness tests could not be conducted. This particularly affected sample P2. It is also known that results at 50 kg may not be directly comparable to those at 10 g because the "indentation size effect" [21, 22] means hardness readings are not always load independent. The microhardness tests for specimens TT and TL from rail P3 reveal the hardness of the WEL to reach 1024 *HV* over this layer, which had a thickness of over 10 μm (see Figure (9c)). The hardness profiles also showed the presence of a stable hardened layer below the surface of the rail underneath the WEL layer. This layer was thought to be formed by work hardening of the steel following deformation by rolling contact.

The hardness of the sub- surface layers was in the range of 250-350 HV for all the samples. Profiles of hardness from the surface down into the visible undeformed material for rail P4 are shown in Figure (9d) for all the samples examined. The Figure shows that increase in hardness of all the samples around 200% with respect to the original hardness at the worn surface. This can be attributed to work hardening. Figure (9e) shows the microhardness measurements from the top surface of the new rail for all the samples examined. The near surface region is softer than the bulk of the material because of the decarburisation layer which located near to the new rail surface.

Shear stress-strain data

Taking the results for shear deformation and hardness, it is possible to construct a stress-strain curve for P1 and P2 rails undergoing plastic deformation at high hydrostatic pressure. Shear deformation can be used directly, but shear stress should be calculated from the hardness readings by using Von Mises shear strain-energy criterion ($k = \sigma_y / \sqrt{3}$) together with Equation (1) [23] which allows the yield stress to be obtained from the hardness readings.

$$\sigma_y = \frac{H}{3} \tag{1}$$

This leads to the following relationship:

$$k = \frac{HV}{3\sqrt{3}} \tag{2}$$

Where *HV* is Vickers hardness in MPa (conversion is required from the value expresses normally in kg/mm^2). Results are plotted for the two rails respectively in Figure (10).
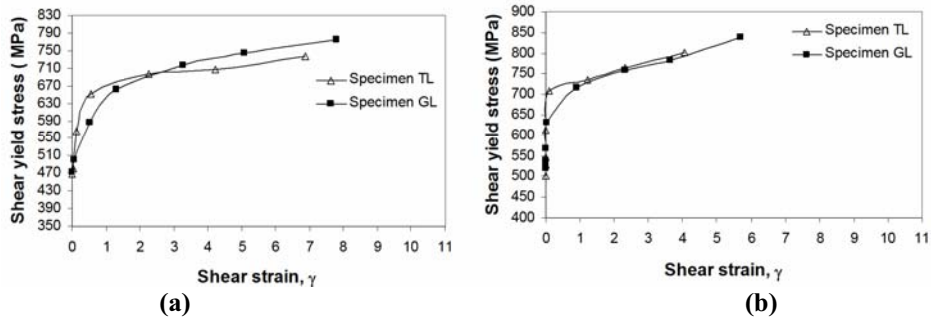
Figure 10: Shear-stress shear-strain curves for (a) rail P1, (b) rail P2.

The value of the equivalent shear strain (γ) corresponding to the shear yield stress at different depth below the worn surfaces for the P3 and P4 rails were calculated by using equation (8). As an approximation, it was assumed that the change of an element of rail material in the lateral and longitudinal directions as shown in Figure (11).
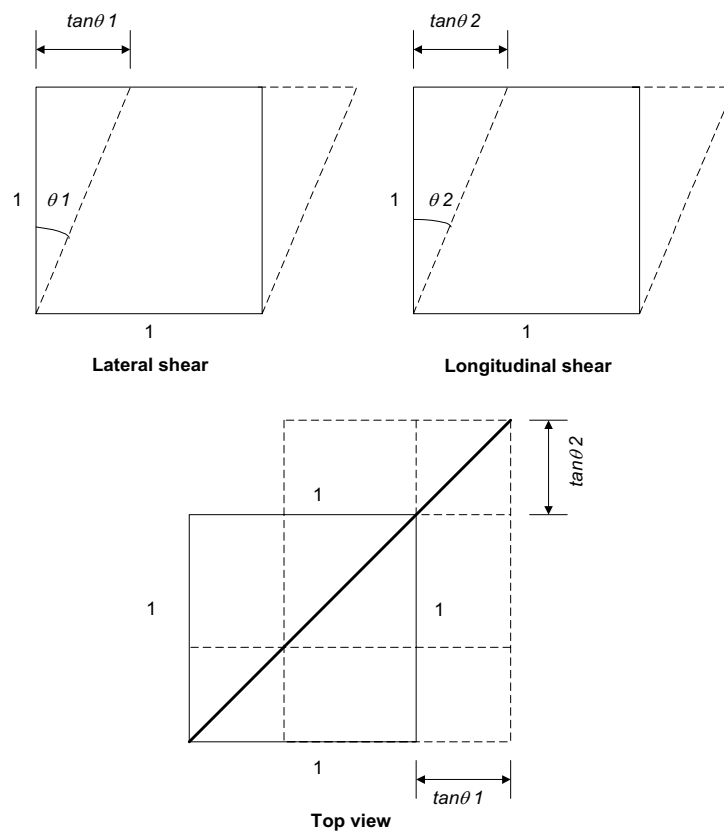
Figure 11: Schematic illustration of the shear strain accumulation in the lateral and longitudinal directions of an element cut from a rail.

Because the shear strain take place in two directions (lateral and longitudinal directions) when the load is applied (wheel pass the rail in railway track). Let us take a small element of isotropic material cut from a rail (see Figure (11). The original shape of the element (shown by the solid lines) is a square having sides of length 1 μm in the x and y directions, respectively. The final shape of the element is shown by dashed lines. The elongation of the element in the lateral direction is $(1 + \tan\theta_1)$ while the elongation of the element in the longitudinal direction is $(1 + \tan\theta_2)$ where θ_1 and θ_2 the angle of the deformed grain boundaries and deformed pearlitic lamellae relative to the normal to the contact surface in the lateral and longitudinal directions respectively.

Thus, the length of the diagonal is given by

$$l_1 = \sqrt{(1+\tan\theta_1)^2 + (1+\tan\theta_2)^2} \tag{3}$$

The original length is:

$$l = \sqrt{1+1} = \sqrt{2} \tag{4}$$

Where

$$\text{Shear strain} = \frac{l_1 - l}{l} = \frac{l_1}{l} - 1 \tag{5}$$

Substituting for l_1 and l in Equation (5) gives:

$$\gamma = \sqrt{\frac{1+\tan^2\theta_1 + 2\tan\theta_1 + 1 + \tan^2\theta_2 + 2\tan\theta_2}{2}} - 1 \tag{6}$$

$$\gamma = \sqrt{1 + (\tan\theta_1 + \tan\theta_2) + \tfrac{1}{2}(\tan^2\theta_1 + \tan^2\theta_2)} - 1 \tag{7}$$

Therefore, the total shear strain of the element is:

$$\gamma = \sqrt{1 + (\gamma_1 + \gamma_2) + \tfrac{1}{2}(\gamma_1^2 + \gamma_2^2)} - 1 \tag{8}$$

Where γ_1 and γ_2 are the shear strain in the lateral and longitudinal directions respectively. These calculations have been done for both rails (P3 and P4) and the shear stress-strain curves for the deformed layer is shown in Figure (12).
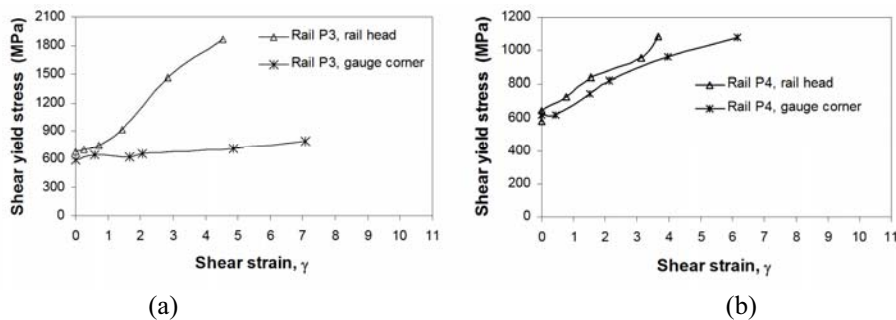
Figure 12: Shear-stress shear-strain curves for (a) rail P3, (b) rail P4.

The shear yield stress of the material changes under rolling-sliding conditions due to strain hardening of the material. As the material strain hardens, the effective shear yield stress increases and the material is able to support larger loads without plastic flow. The result is an increase in the shakedown limit. The material hardens very rapidly with increased strain for rails P1, P2 and P4, but for rail P3 there is a high maximum of work hardening at top longitudinal (TL) sample. This is because of the high hardness of the white etching layer (WEL) which lies on top of the rail surface.

DISCUSSIONS

In rail-wheel contact, both rolling and sliding occur in the contacting zone. On straight track, the wheel tread is in contact with the rail head, but in curves, the wheel flange may be in contact with the gauge corner of the rail. Due to the conicity of the wheel profile, flanging results in a large sliding motion in the contact [24]. This may explain the reason behind the difference in plastic deformation between rail head and rail edge, which has also been reported in the full-scale tests [25]. It has been shown in Figures. (5 and 7b) that the four used rails were subjected to different shear stress levels according to their depth below the surface, where the surface material was subjected to the maximum shear stress. These shear stresses will produce a shear strain, which decreases with the depth. The rails surface will see maximum strain. This leads to strain hardening, the maximum of which is also at the surface. Kapoor et al. [20] reported that surface roughness is the probable cause of the thin, plastically deformed surface layer observed in rails. The rail and wheel make contact at asperities, the widths of such contacts vary but are typically on the order of a few microns, and the pressures at such contacts far exceed the pressure that would arise from a smooth contact. Therefore, not only are the pressures at asperity contacts likely to exceed the shakedown limit, but the maximum shear stresses will occur at depths within a few microns of the surface.

In all cases, it has been clarified that the plastic deformation region extends from the gauge corner surface side to the rail head surface side. It is well known that work hardening occurs as a result of dislocation interaction; therefore, the degree of hardening is a function of dislocation density. According to previous study by Ueda et al. [26], the reason why the maximum hardness of the rolling contact surface of pearlitic steels rises is considered to be as follows: the rail-wheel contact introduces strain into the ferrite phase and at the same time produces fractures in the cementite phase beneath the contact surface. Repeated rolling contact concentrates strain in the ferrite phase that is lower in hardness than the fractured cementite. The strain concentration forms many dislocations in the matrix ferrite, and promotes dislocation hardening and grain refinement in the matrix ferrite. As a result, the matrix ferrite is strengthened by dislocation hardening and grain refinement. The work hardening rate of the contact surface rises as the carbon content of the pearlitic steels increases. The results show different work hardening for the four used rail steels which is containing different carbon content. Tarui et al. [27] reported that when a high carbon wire is cold-drawn, the cementite phase in the pearlite structure is decomposed, and the carbon of the cementite phase is dissolved into the matrix ferrite phase, and the ferrite phase is strengthened by the solid solution of carbon. They report that the rail-wheel contact surface is subjected to a more severe processing condition than that of wire drawing, and the cementite phase is presumed to decompose by the rolling contact. Therefore, the increased amount of carbon dissolving into the matrix ferrite as the cementite density

increases is considered to be one of the factors responsible for the raised work hardening rate of the rolling contact surface.

It was observed that thin white surface layer, frequently called white etching layer (WEL), with 10 to $40 \, \mu m$ thicknesses. See Figure (6b) it may be produced by the accumulation of plastic deformation. The surface white etching layer has a close relationship to plastic deformation, and also regarded as dissolution of cementite during severe plastic deformation, and transformation of the supersaturated $\alpha - Fe$ into martensitic structure [28]. The WEL seems to reach hardness values up to ~1040 HV. This high hardness can be linked to the presence of martensite [29]. Beneath this layer a region of deformed pearlite is observed. The hardness of this deformation region is almost 1.5 times the bulk hardness. The increase in the hardness depends on the rise in the work hardening of the contact surface as the carbon content increases. The structure below the white layer exhibits deformed and broken cementite lamellae. The hardening process is caused by decreased interlamellar spacing, which sufficiently has increased hardness and yield stress of the material.

CONCLUSIONS

In this study, optical micrograph observations were used to investigate the plastic deformation near the surface of the worn rails following service. In addition, the hardness distribution in this region, very close to the rail surface, was determined. Since heavy deformation was observed near to the worn surface, microhardness measurements were carried out along these surfaces. From the results of present study the following conclusions can be drown:

- The plastic deformation is highly concentrated producing a narrow shear zone with depth of approximately 50 to 180 μm across the surface of the rails due to micro roughness and 1-10 mm due to the bulk contact.
- The optical micrograph of the near surface layer of the worn rail shows different deformation between the four used rails. This could be related to different strength, structural parameter, Carbon content and service operation conditions.
- The thickness of the deformation layer is different in different locations of the same rail. This layer is deeper at the gauge corner of the rail than on the rail head.
- Strain hardening is maximal at the surface of the rails and then decreases in a non-linear fashion. The surface hardness reaches a value ≈ 1.8 times that of the bulk material for all pearlitic rail steels examined.
- The microscopy study of rail P3 showed a White Etching Layer (WEL) on the worn surface. The hardness of the WEL reached 1040 HV and the thickness varies between $10 - 40 \, m\mu$.

REFERNCES

[1] Alpas, A.T., Hu, H. and Zhang, J., "Plastic deformation and damage accumulation below the worn surfaces", Wear, 1993, 162, 88-195.

[2] Dautzenberg, J. H. and Zaat, J. H. Quantitative determination of deformation by sliding wear. Wear, 1973, 23, 9-19.

[3] Bower, A. F. and Johnson, K. L., "Plastic flow and shakedown of the rail surface in repeated wheel-rail contact", Wear, 1991, 144, 1-18.

[4] Johnson, K. L., "The mechanics of plastic deformation of surface and subsurface layers in rolling and sliding contact", Material science forum: The role of surface zone in wear of materials, Trans Tech Publications, 1988, 33-40.

[5] Olver, A. V., Spikes, H. A., Bower, A. F. and Johnson, K. L., "The residual stress distribution in a plastically deformed model asperity', Wear, 1986, 107, 151-174.

[6] Rigney, D. A., Naylor, M. G. S. and Divakar, H., "Low energy dislocation structures caused by sliding and particle impact", Mater. Sci. Eng., 1986, 81, 409-425.

[7] Kapoor, A. "A re-evaluation of the life to rupture of ductile metals by cyclic plastic strain", Fatigue and fracture in engineering materials and structures, 1994, 17 (2), 201-219.

[8] Kapoor, A. "Wear by plastic ratchetting", Wear, 1997, 212, 119-130.

[9] Kapoor, A. and Franklin, F. J., "Tribological layers and wear of ductile materials", Wear, 2000, 245, 204-215.

[10] Franklin, F. J., Widiyarta, I. and Kapoor, A. , "Computer simulation of wear and rolling contact fatigue", Wear, 2001, 251, 949-955.

[11] Fletcher, D. I., Franklin, F. J. and Kapoor, A., "Image analysis to reveal crack development using a computer simulation of war and rolling contact fatigue", fatigue and fracture of engineering materials and structures, 2003, 26, 957-967.

[12] Baumann, G., Knothe, K. and Fecht, H. J., "Surface modification, corrugation and nanostructure formation of high speed railway tracks", Nanostructured Materials, 1997, 9, 751-754.

[13] Zhang, B., Liu, Y., Shen, W., Wang, Y., Tang, X. and Wang, X., "A study on the behavior of adiabatic shear bands in impact wear", Wear, 1996, 198, 287-292.

[14] Zhang, B., Shen, W., Liu, Y. and Zhang, R. , "Some factors influencing adiabatic shear banding in impact wear", Wear, 1998, 214, 259-263.

[15] Lojkowski, W., Djahanbakhsh, M., Burkle, G., Gierlotka, S., Zielinski, W. and Fecht, H. J., "Nanostructure formation on the surface of railway tracks", Materials science and engineering, 2001, A 303,197-208.

[16] Frantz, J., http://www.acclab.helsinki.fi/~frantz/software/g3data.php, Software under the GNU General Public License (30/07/2006).

[17] Tyfour, W. R., Beynon, J. H. and Kapoor, A., "Deterioration of rolling contact fatigue life of pearlitic rail steel due to dry-wet rolling-sliding line contact', Wear, 1996, 197, 255-265.

[18] Cimenoglu, H., "Subsurface characteristics of an abraded low carbon steel', Wear, 1997, 210, 204-210.

[19] Sachs, K., "Decarburization: definition and measurement", 1st international Conference on Decarburization, Sheffield, UK, 24th-27th September, 1969.

[20] Kapoor, A., Franklin, F. J., Wong, S.K. and Ishida, M., "Surface roughness and plastic flow in rail wheel contact", Wear, 2002, 253, 257-264.

[21] Sangwal, K., "On the reverse indentation size effect and microhardness measurement of solids", Materials Chemistry and Physics, 2000, 63, 145-152.

[22]   Sangwal, K, Surowska, B. and Blaziak, P., "Analysis of the indentation size effect in the microhardness measurement of some cobalt-based alloys", Materials Chemistry and Physics, 2002, 77, 511-520.

[23]   Tabor, D. , The hardness of metals, 1951, Oxford University Press

[24]   Olofsson, U. and Nilsson, R., "Surface cracks and wear of rail: a full-scale test on a commuter train track", Proc. Inst. Mech. Engrs, J. Rail and Rapid Transit, 2002, 216, 249-264.

[25]   Olofsson, U. and Telliskivi, T., "Wear, plastic deformation and friction of two rail steels-a full-scale test and a laboratory study", Wear, 2003, 254, 80-93.

[26]   Ueda, M., Uchino, K. and Kobayashi, A., "Effects of carbon content on wear property in pearlitic steels", Wear, 2002, 253,107-113.

[27]   Tarui, K., Maruyama, N., Shigesato, G. and Tashiro, H., "Zairyou-to- Process, 1998, 11, 1327.

[28]   Baumann, G., Fecht, H. J. and Liebelt, S., "Formation of white-etching layers on rail treads", Wear, 1996, 191, 133-140.

[29]   Pyzalla, A., Wang, L., Wild, E. and Wroblewskoi, T., "Changes in microstructure, texture and residual stresses on the surface of a rail resulting from friction and wear", Wear, 2001, 251, 901-907.

NOTATION

H	hardness
HV	Vickers hardness
k	shear yield stress
l	the original length
l_1	the length of the diagonal
θ	the angle of the deformed grain boundaries and deformed pearlitic lamellae relative to the normal to the contact surface
θ_1, θ_2	the angle of the deformed in the lateral and longitudinal directions respectively
γ_1, γ_2	the shear strain in the lateral and longitudinal directions respectively
γ_p	total accumulated plastic shear strain
γ_c	critical plastic shear strain
σ_y	yield stress